Fast photochronoamperometry of photosynthetic complexes for biosensors and electron transport studies

Manuel López-Ortiz[1,2], Ricardo A. Zamora[1,2], Vikas Remesh[3], Chen Hu[4], Roberta Croce[4], Niek van Hulst[3,5], Pau Gorostiza[1,2,5,*]

1. Institute for Bioengineering of Catalonia (IBEC), the Barcelona Institute for Science and Technology. Baldiri Reixac 15-21, Barcelona 08028

2. Network Biomedical Research Center in Biomaterials, Bioengineering and Nanomedicine (CIBER-bbn).

3. The Institute of Photonic Sciences (ICFO), The Barcelona Institute of Science and Technology, 08860 Castelldefels (Barcelona), Spain.

4. Department of Physics and Astronomy and Institute for Lasers, Life and Biophotonics , Faculty of Sciences , Vrije Universiteit Amsterdam , De Boelelaan 1081 , 1081 HV Amsterdam , The Netherlands.

5. Catalan Institution for Research and Advanced Studies (ICREA), 08020 Barcelona Spain

(*) Correspondence to pau@icrea.cat

Abstract

Photosynthetic reactions in plants, algae and cyanobacteria are driven by photosystem I and II complexes, which specifically reduce or oxidize partner redox biomolecules. Photosynthetic complexes can also bind synthetic organic molecules, which inhibit their photoactivity and can be used both to study the electron transport chain, and as herbicides and algicides. Thus, their development, characterization and sensing bears fundamental and applied interest. Substantial efforts have been devoted to developing photosensors based on photosystem II to detect compounds that bind to the plastoquinone sites of the complex. In comparison, photosystem I based sensors have received less attention and could be used to identify novel substances displaying phytotoxic effects, including those obtained from natural product extracts. We have developed a robust procedure to functionalize gold electrodes with photo- and redox-active photosystem I complexes based on transparent gold and a thiolate self-assembled monolayer, and we have obtained reproducible electrochemical photoresponses. Chronoamperometric recordings with millisecond resolution have allowed to measure photocurrents in the presence of the viologen derivative paraquat. We have modeled their time course to identify the main electrochemical processes and limiting steps in the electron transport chain. Our results allow isolating the contributions from photosystem I and the redox mediator, and evaluating photocurrent features (spectral and power dependence, fast transient kinetics) that could be used as a sensing signal to detect other inhibitors and modulators of photosystem I activity.

1. Introduction

In nature, photosynthetic reactions are driven by two multi-protein complexes: Photosystem I (PSI) and Photosystem II (PSII). Both photosynthetic complexes have oxidoreductase functions capable of specifically reducing or oxidizing partner biomolecules. Despite their high specificity

towards natural redox biomolecules like cytochromes, plastocyanin and plastoquinone, both PSI and PSII can also bind synthetic organic molecules, which inhibit their photoactivity [REF1]. These compounds can be used both to dissect the photosynthetic electron transport chain, and as herbicides and algicides, and thus their development, characterization and sensing bears fundamental and applied interest. In the case of PSII, herbicides compete for the binding sites of the plastoquinone (Q_A and Q_B). The binding of compounds such as triazine, triazinone, pyridazinone, benzothiadiazinone, nitrile, phenylpyridazine, and phenol derivatives at the Q_B site, inhibits the electron transfer between primary quinone site Q_A (D_2 subunit) and Q_B site in the D_1 subunit [REF2]. Due to this affinity between PSII and this type of herbicides, many studies have been focused on developing PSII-based photosensors for the detection of this type of herbicides.

Synthetic compounds that interact with PSI have also been developed and used as herbicides. They are generally referred to as PSI electron diverters. These molecules bind at the PsaC subunit of PSI, competing with the physiological redox partner ferredoxin (Fd) to uptake the photogenerated electrons from the F_B cluster, thereby preventing the generation of reducing power (NADPH) that is necessary to maintain normal cell function. Bipyridillium compounds of the Quat family (Paraquat, PQ; Diquat, DQ, and Ciperquat CQ) are viologen derivatives that can interact with PSI and prevent its normal oxidation via Fd [REF3-4]. In particular, PQ (methyl viologen) has been extensively used in bioelectrochemical studies and in biohybrid devices as an artificial electron acceptor (redox mediator) of PSI photoactivated electrons.

In PSI, the structural basis of photo-generation and separation of electron-hole pairs is relatively well understood [REF5-6]. It acts as a photodiode that upon illumination shuttles electrons in one direction through its embedding membrane. Photo-excited electrons occupy high energy states at the chlorophyll special pair site (P700), where the separation from the vacancy states (holes) is initiated by means of a fast (10^{-8}–10^{-7} s) electron transfer (ET) cascade[REF7]. The process involves an electron transport chain of several protein cofactors, from P700 located at the luminal side of the complex towards the terminal iron sulfur cluster F_B at the stromal surface, which is the electron donor site to Fd and PQ. The state resulting from electron photoexcitation, $P700^+/F_B^-$ has a recombination rate orders of magnitude smaller than charge transfer rates through protein's electron transport chain, making of PSI a very efficient photo-conversion system with a quantum yield near 100% [REF8]. As such, the PSI photoconversion capacity can be exploited to and act as photoactive material in a photoelectrochemical (PEC) sensors [REF9] if proper electrode functionalization can be achieved.

Increasingly efficient PSI biohybrid photoanodes have been developed by improving protein complex functionalization, stability, enhancing ET between electrode and PSI with mediators and avoiding short-circuiting recombination processes.[REF10] Altogether these achievements have led to a 10^5-fold increase of photocurrent output from first reported photocurrents of 0.1 $nA \cdot cm^{-2}$ and 10 $\mu A \cdot cm^{-2}$[REF11-12]. However, despite these achievements and notwithstanding that PSI has better protein stability, quantum yield, and more direct electronic coupling than PSII, to our knowledge the use PSI as photoactive material for PEC bionsensing has not been reported.

In order to explore this possibility, we based our design on screen-printed gold transparent electrodes (AUTR10 Dropsens), which can be customized and coupled to a variety of measurement setups. In particular, we functionalized trasparent gold electrodes with a thiolated

self-assembled monolayer (SAM) prior to depositing the purified PSI protein complexes. The hydroxyl-terminated film interacts preferentially with the positively-charged luminal side of PSI and enables to orient the PSI P700 site towards the electrode, thereby exposing the F_B site to the bulk solution [REF López-Martínez 2019]. This arrangement allows transferring electrons from F_B^- to acceptors in solution like PQ, which acts as a redox mediator. PQ eventually short-circuits photo-generated charges back to the electrode, giving rise to a transient photocurrent characteristic of PSI-PQ-electrode ET processes [REF13-14]. The photoelectrochemical behavior of PQ in solid PSI-based biohybrid systems has only been characterized with a temporal resolution in the range of seconds. However, recording transient photoresponses with submillisecond resolution [in well-defined PSI monolayer arrangements] and modeling the underlying photoelectrochemical processes are essential steps to understand their mechanisms, and to determine the necessary conditions for using PSI as a biophotosensor device, as well as to improve its performance. Thus, the aims of this work are (1) setting up a reproducible method to functionalize gold electrodes with photo- and redox-active PSI complexes, (2) using fast chronoamperometric recordings to measure photocurrent responses in the presence of PQ, and (3) modeling the time course of the photoresponses as a means to identify the leading electrochemical processes and limiting steps in the ET chain. Our results allow evaluating photocurrent features (spectral and power dependence, fast transient kinetics) that could be used as a sensing signal to detect inhibitors and modulators of PSI activity, including viologen-derived herbicides. We also modeled photocurrent transient signal to deconvolute contributions from PSI and redox mediator.

2. Results

2.1 System characterization: Steady photocurrent power & spectral dependence

Upon light irradiation, PSI-SAM functionalized electrodes in buffer solution containing PQ, exhibit a transient photocurrent peak of several µA·cm^{-2} followed by a steady photocurrent of around 10 nA·cm^{-2}. To characterize the photoactive layer photo-conversion performance, we quantify the steady photocurrent output under irradiation of a broadband Ti:Sa-Laser. Acousto-optic modulation was employed to control excitation wavelength and power, that was measured in PEC location with a digital power-meter. In the investigated power range, we observe a linear photocurrent response with monochromatic light power (Figure 1A). The steady photocurrent spectrum (Figure 1B) reveals a photoconversion profile that follows PSI absorption spectra measured in bulk. This result suggest that PSI molecules are responsible for photoconversion ability of the electrode.

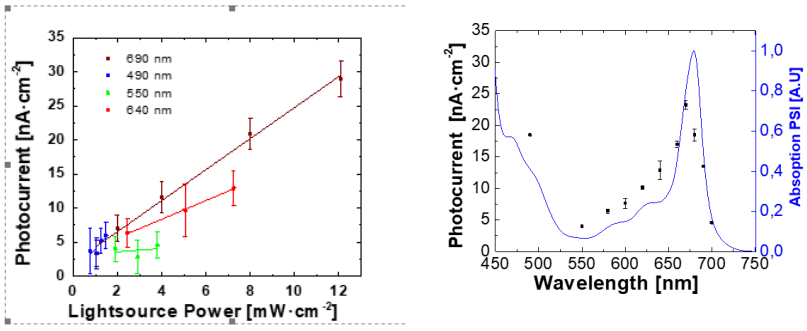

Figure 1: PSI photocurrent responses as a function of illumination wavelength and power. (a) Photocurrent increases linearly response with monochromatic light power. (b) The photocurrent

magnitude as a function of wavelength (left axis) follows a similar profile than the PSI absorption spectra measured in bulk solution using a spectrophotometer (right axis).

2.2 Chopped Light Voltammetry: Transient photocurrent dependence with sample potential

The redox behaviour of PQ can be evidenced in a cyclic voltammetry (CV) experiment, in which potential measurements were performed with respect to the printed/built-in silver pseudo reference electrode (Ag/AgCl). In the CV shown figure 2A (black trace), the reduction peak ($PQ^{2+} \rightarrow PQ^{+}$) can be observed at –900 mV/Ag and the corresponding oxidation peak ($PQ^{+} \rightarrow PQ^{2+}$) at –815 mV/Ag for an argon purged physiological buffer solution (Phophate Saline Buffer, PBS 50 mM pH 7.4) containing 125 µM of PQ in transparent gold micro-electrode functionalized with 6-mercapto hexanol SAM. PSI incubation, shifts the PQ's redox peaks to –765 and –700 mV/Ag respectively indicating an enhanced ET with the electrode (Figure 2A, blue trace). The widening of the CV for PQ in SAM-PSI compared to SAM microelectrode indicates an increased electrode capacity that can be atributed to PSI complexes absortion. Sample irradiation cycles with an LED (λ 690 nm, 375 mW) give rise to photocurrent peaks as sample potential approaches PQ redox potentials (Figure 2A, red trace). In Figure 2B, we display chopped light linear voltammetry ranging from –450 mV/Ag to –900 mV/Ag, where sample irradiation has been indicated with red marker. A sudden increase in current is observed upon light illumination accompanied by a negative peak that follows the end of the illumination cycle. Transient current amplitude and characteristic time is remarkably affected by sample electrode potential, vanishing around the redox mid-point of PQ in the sample $V_{PQ} \sim$ –650 mV and eventually inverting the sign of light switching current transients for sample potentials bellow the redox midpoint.

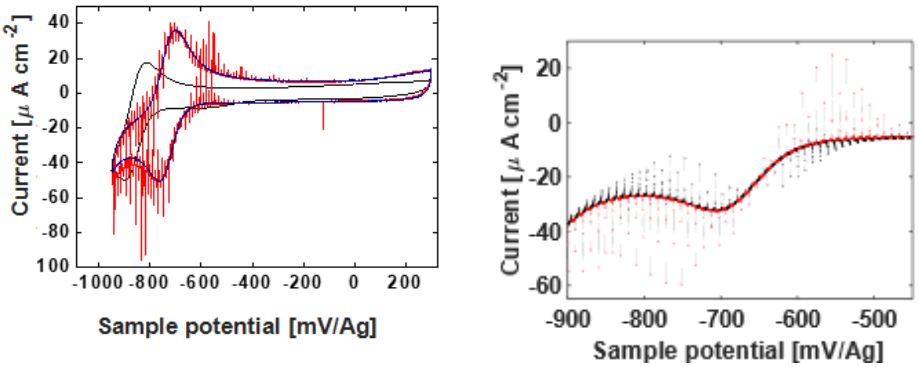

Figure 2: PSI photocurrent responses as a function of electrode potential. (A) Cyclic voltammetry of Au-SAM transparent electrodes prior to (grey trace) and after incubation (blue trace) in PSI complex solution and wash (potential scan rate 50 mV/s). Au-SAM-PSI irradiated LED (690 nm, 340 mW photoswitch rate 50 ms, red trace). (B) Linear scan voltammetry of Au-SAM-PSI irradiated LED (690 nm, 340 mW photoswitch rate 300 ms). Illumination and dark conditions are indicated with red and black markers, respectively.

2.3 Fast chronoamperometry: Empirical characterization with double exponential function

To further investigate the PSI-PQ system's current transient behavior under illumination, we perform chrono-amperometry experiments for a set of fixed sample potentials (Figure 3A). This operation mode allowed a higher sampling rate (100 kHz) and 30 ms LED switching cycles. We observed a remarkable dependence with applied sample potential in the magnitude, sign, and time course of the photoresponses, upon turning on and off LED. Transient photocurrents could

be fit empirically using two exponential functions of opposite sign, yielding four fitted parameters for off-on (A_{ON+}, A_{ON-}, τ_{ON+}, τ_{ON-}) and 4 for on-off transitions (A_{OFF+}, A_{OFF-}, τ_{OFF+}, τ_{OFF-}).

$$j(t) = A_+ \cdot \exp(-t/\tau_+) - A_- \cdot \exp(-t/\tau_-) \qquad (1)$$

An example fit is presented in Figure 3B, and the obtained parameters are shown in Figure 2C as a function of the electrode potential. Fast off-on transition with $1/\tau_{ON+}$ 5 ms^{-1} for $V < V_{PQ}$ switches to slower process with $1/\tau_{ON+}$ ~ 1 ms^{-1} for $V > V_{PQ}$. A_+ and A_- amplitudes for both on-off/off-on transitions have similar magnitude ranging between 1 and 8 uA and opposite sign. Bimodal fit behavior describes two opposite kinetic processes.

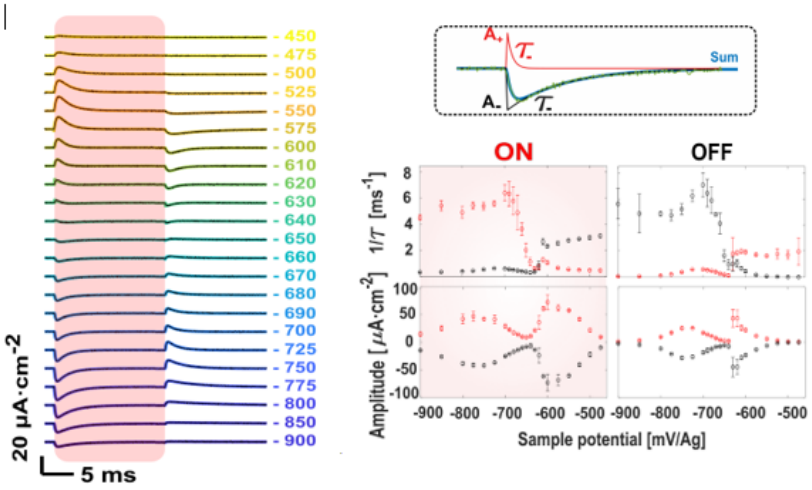

Figure 3: PSI photoresponse kinetics and empirical fits. (A) Fast photochronoamperometry traces of PSI-SAM-Au functionalized electrodes at different potentials (between -400 and -900 mV versus Ag electrode) and sampled at 100 kHz (or 10 µs resolution). Red box indicates the period of illumination with a 690 nm LED. (B) Each photocurrent trace could be fit (non-linear least squares method) with the sum of two exponential decay functions having different amplitudes and decay times (A_{ON+}, A_{ON-}, τ_{ON+}, τ_{ON-}, A_{OFF+}, A_{OFF-}, τ_{OFF+}, τ_{OFF-}). Parameters obtained from fitting the traces of panel (A) as a function of the potential applied to the PSI-SAM electrode.

2.4 Kinetic model: Describe mediator and PSI cofactors concentration

The bimodal results of Figure 3 can be fitted by a kinetic model describing the electronic exchange between the electrode and PSI cofactor P700, reduced and oxidized PQ and between F_B cofactor and the oxidized form of the mediator PQ^{2+} as well as the photoexcitation and recombination rates for PSI. Similar kinetics models that describing PSI photocurrents have been published previously (REF14-15-16-17-18). These models consider diffusion, PSI excitation and recombination, mediator-PSI electron exchange, and mediator-electrode. In our system (SAM-PSI-PQ) photocurrent generation is dominated by the electron exchange of the mediator with the electrode. Electrode's potential determines the generation rates of oxidized/reduced PQ species that eventually reach a steady state of constant relative concentration. This balance is altered by the sudden increase in PQ^+ produced by the ET from PSI to PQ^{2+}. Transient photocurrents are described by a model that does not consider the mediator's diffusion (Figure 4A and equations 1-8 in supplementary information). To assume this simplification in the model,

the thickness of the SAM-PSI monolayer in the system should be less than the typical diffusion length. This diffusion length can be calculated as $L = (2DT)^{1/2}$, where T is a lower bound of the observed characteristic time of the PSI-PQ system (1 ms). Considering a value of the PQ diffusion coefficient of the 10^{-6} cm^2/s, the diffusion length obtained is 0.5 um, which is much less than the 7 nm thickness of a reported Au-SAM-PSI monolayer [REF19]. To build the kinetic model (supplementary information), the same set of parameters for the constants for excitation, recombination, was used to adjust all the photocurrents registered for the different potentials evaluated. PQ-electrode constant rates PQ depend on the potential according to the equation described in the supplementary file. Under illumination conditions (t [0-15] ms), the excitation constant is an adjustable parameter of the model, while it has a null value in the absence of illumination (t [15-30] ms).

The kinetic model output provides access to the relative concentrations of PQ^+/PQ^{2+} (Figure 4B, top row), excited $P700^+/P700$ and F_B^-/F_B (Figure 4B, middle row) and contributions to the current from PQ^{2+}, PQ^+, and $P700^+$ (Figure 4B, bottom row). The PQ^+/PQ^{2+} stationary concentration decreases (for t=0 and $t\rightarrow\infty$) as sample potential is increased from $V < V_{PQ}$ to $V > V_{PQ}$ modulating the rate constants for $PQ^{2+} \rightarrow PQ^+$ and $PQ^+ \rightarrow PQ^{2+}$. We observe that while light irradiation (starting at t=0) increases PQ^+/PQ^{2+} relative concentration for all potentials, light-induced PQ^+ increment with respect to stationary concentration is more pronounced for $V > V_{PQ}$. F_B^-/F_B PSI redox cofactors relative abundance is higher than $P700^+/P700$ for $V < V_{PQ}$. This effect can be due to low PQ^{2+} concentration limiting the electron uptake from F_B^-.

On the other hand, for $V > V_{PQ}$, where PQ^{2+} is favored, higher $P700^+$ and lower F_B^- relative concentrations indicate that the electrons are drained from F_B^- by the majority PQ^{2+} forming PQ^+. Charged drained by PQ^+ is, in turn, recombined in the electrode giving rise to a positive current that cancels out the $P700^+$ to electrode negative current (Figure 4B, bottom row). Both currents are larger in magnitude than the transient currents observed in the case of $V < V_{PQ}$. The redox mediator couple $PQ^{2+}|PQ^+$ shuttles electrons to the electrode, canceling out the PSI photogenerated charges resulting in a stationary state with a negligible current. The increased PQ^+ generation rate produced by F_B^- reduction of PQ^{2+} shifts the electrochemical equilibrium to a new stationary state. The observed transient currents are due to the shift between these stationary regimes. The change of regime is governed by the $PQ^+|PQ^{2+}$ electron exchange with the electrode resulting in the observed transient currents. For $V < V_{PQ}$, where the $e^- + PQ^{2+} \rightarrow PQ^+$ is the dominant rate, making the transient current is negative, while for $V > V_{PQ}$, the favored process is $PQ^+ \rightarrow PQ^{2+} + e^-$ producing positive transient currents.

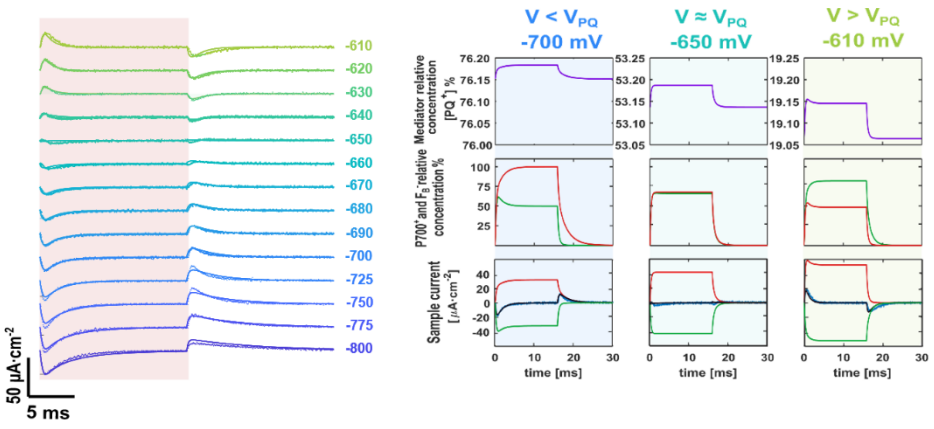

Figure 4: Kinetic model fit. (A) On (red shaded area) and off kinetic model fit of transient photcurrents. (B) PQ^+ relative concentration for V=-700 mV/Ag (blue, left), -650 mV/Ag (aquamarine, middle) and –610 mV/Ag (light green, right) (top row). The same potentials, indicated with color boxes are applies to middle and bottom rows. $P700^+$ (green trace) and F_B^- (red trace) relative concetrations (middles row). Components of modeled transient current from PQ^+/PQ^{2+} (red), $P700^+$ (green), total modeled current (blue) and experimental data (black)(bottom row).

2.5. Considerations for sensor design and optimization

We have found several key advantages of transparent microelectrodes to sense PSI mediators like PQ: (1) they can operate with 10-100 μl of sample volume (corresponding to 1-10 nmol of analyte at 100 μM); (2) they produce faster photocurrent transients that require shorter integration time to be detected and would lead to faster responding sensors; (3) they are ready to use and help reducing variability in electrode preparation; (4) backside illumination is reproducible at the sensing surface, not subject to solution effects (absorption, scattering) and favors sensor robustness and compatibility with spectro-electrochemical measurements (UV-VIS, Raman, NIR). Regarding the potential and illumination applied to the sensor surface, the PQ^+/PQ^{2+} ratio is increased by light in both potential ranges: (1) for $V < V_{PQ}$, the process is limited by regeneration rate of PQ^{2+}, and (2) for $V > V_{PQ}$, the process is limited by direct ET from the electrode to $P700^+$. The excess of species (F_B^- for $V < V_{PQ}$ and $P700^+$ for $V > V_{PQ}$) is regenerated when light is turned off, leading to transient current of opposite sign. This behavior suggests that increasing the flickering frequency and/or alternating the potential may provide higher detection sensitivity, accuracy, and allow testing smaller analyte volumes and concentrations. Current efforts in the laboratory are directed at overcoming the limitations in the coupling of PSI to the electrode by improving the orientation and electrical connection of the complex [REF10-20]. This will allow screening a diversity of analytes, including synthetic herbicides, analog compound libraries, redox protein partners and modulators, and most interestingly, extracts of natural products to evaluate their use for sustainable weed control. Note that the use of a natural photosynthetic complex as the sensing element also avoids toxic components and potentially allows regeneration of the sensing surface, as shown in biophotovoltaic devices based also on PSI [REF20]

4. Conclusions

We have prepared electrodes functionalized with a SAM and photosystem I that allow sensing the presence of PQ in physiological conditions using time-resolved measurements at millisecond resolution. We have characterized the power and steady photocurrent spectra response of the modified electrode at different excitation wavelengths. The photocurrent spectra's correlation with the PSI absorption spectrum corroborates that in our biophotoelectrochemical sensor system, the photoconversion process is mediated by PSI. The compact sensor setup built is based on transparent gold microelectrodes coated with fresh SAM, and PSI layers, with the built-in red LED behind a transparent electrode. Taking advantage of the widely characterized redox interaction between PSI and the herbicide PQ, our work represents the first systematic study on fast photocurrent transients in the millisecond range in this type of system. The observed transients can be fitted with a double exponential function, which indicates that both the PSI-mediated photoconversion process and the PQ recombination process can be clearly differentiated. We observe a change of behavior near the PQ redox potential. The characterization of the transients generated by PSI and PQ is relevant to design sensors with shorter integration times for electrochemical determinations. The kinetic model introduced in

this work allows the identification and electrochemical evaluation of the different species involved in the detection process. This is an essential step to improve the performance of the photosystem I based sensor and to use it for the identification of other relevant inhibitors.

Acknowledgements:

This research received funding from the Barcelona Institute of Science and Technology (Ignite program), from the Agency for Management of University and Research Grants (AGAUR of the Generalitat de Catalunya (CERCA Programme; 2017-SGR-1442 project; RIS3CAT plan), Fonds Européen de Développement Économique et Régional (FEDER) funds, Ministry of Economy and Competitiveness (grants CTQ2016-80066-R and PID2019-111493RB-I00). R.Z. was supported by Becas Chile fellowship 74190117 from the government of Chile.

References

(1) Ricardo, R.; Luiz, J.; Luiz, W. Photosynthetic Inhibitors. Applied Photosynthesis 2012, DOI: 10.5772/26959.

(2) Lambreva, M. D.; Russo, D.; Polticelli, F.; Scognamiglio, V.; Antonacci, A.; Zobnina, V.; Campi, G.; Rea, G. Curr. Protein Pept. Sci. 2014, 15, 285−295.

(3) Swainsbury, D. J. K.; Friebe, V. M.; Frese, R. N.; Jones, M. R. Evaluation of a Biohybrid Photoelectrochemical Cell Employing the Purple Bacterial Reaction Centre as a Biosensor for Herbicides. Biosens. Bioelectron. 2014, 58, 172−178.

(4) Giustini, M.; Autullo, M.; Mennuni, M.; Palazzo, G.; Mallardi, A. Polymer-Photosynthetic Protein Multilayer Architectures for Herbicide Optical Detection. Sens. Actuators, B 2012, 163 (1), 69−75.

(5) Zhang, W.; Liu, M.; Zhang, P.; Yu, F.; Lu, S.; Li, P.; Zhou, J. Effects of Paraquat on Photosynthetic Pigments, Antioxidant Enzymes, and Gene Expression in Chlorella Pyrenoidosa under Mixotrophic Compared with Autotrophic Conditions. Arch. Environ. Contam. Toxicol. 2014, 67 (4), 593−600.

(6) Forouzesh, A.; Zand, E.; Soufizadeh, S.; Samadi Foroushani, S. Classification of Herbicides According to Chemical Family for Weed Resistance Management Strategies-an Update. Weed Res. 2015, 55 (4), 334−358.

(7) Croce, R.; van Amerongen, H. Light Harvesting in Oxygenic Photosynthesis: Structural Biology Meets Spectroscopy. Science 2020, 369 (6506), eaay2058.

(8) Jumper, C. C.; Rafiq, S.; Wang, S.; Scholes, G. D. From Coherent to Vibronic Light Harvesting in Photosynthesis. Curr. Opin. Chem. Biol. 2018, 47, 39−46.

(9) Brettel, K.; Leibl, W. Electron Transfer in Photosystem I. Biochim. Biophys. Acta, Bioenerg. 2001, 1507 (1−3), 100−114.

(10) Nelson, N. Plant Photosystem I - The Most Efficient Nano-Photochemical Machine. J. Nanosci. Nanotechnol. 2009, 9 (3), 1709−1713.

(11) Shu, J.; Tang, D. Recent Advances in PhotoelectrochemicalSensing: From Engineered Photoactive Materials to Sensing Devices and Detection Modes. Anal. Chem. 2020, 92 (1), 363−377.

(12) Robinson, M. T.; Gizzie, E. A.; Mwambutsa, F.; Cliffel, D. E.; Jennings, G. K. Mediated Approaches to Photosystem I-Based Biophotovoltaics. Current Opinion in Electrochemistry 2017, 5 (1), 211−217.

(13) Zhao, F.; Ruff, A.; Rögner, M.; Schuhmann, W.; Conzuelo, F. Extended Operational Lifetime of a Photosystem-Based Bioelectrode. J. Am. Chem. Soc. 2019, 141 (13), 5102−5106.

(14) Terasaki, N. PS-I and PS-II on Electrodes for Energy Generation and Photo-Sensor. Lecture Notes in Energy 2016, 32, 419−449.

(15) Ko, B. S.; Babcock, B.; Jennings, G. K.; Tilden, S. G.; Peterson, R. R.; Cliffel, D.; Greenbaum, E. Effect of Surface Composition on the Adsorption of Photosystem I onto Alkanethiolate Self-Assembled Monolayers on Gold. Langmuir 2004, 20 (10), 4033−4038.

(16) Ciobanu, M.; Kincaid, H. A.; Lo, V.; Dukes, A. D.; Kane Jennings, G.; Cliffel, D. E. Electrochemistry and Photoelectrochemistry of Photosystem I Adsorbed on Hydroxyl-Terminated Monolayers. J. Electroanal. Chem. 2007, 599 (1), 72−78.

(17) Zhao, F.; Wang, P.; Ruff, A.; Hartmann, V.; Zacarias, S.; Pereira, I. A. C.; Nowaczyk, M. M.; Rögner, M.; Conzuelo, F.; Schuhmann, W. A Photosystem i Monolayer with Anisotropic Electron Flow Enables Z-Scheme like Photosynthetic Water Splitting. Energy Environ. Sci. 2019, 12 (10), 3133−3143.

(18) Manocchi, A. K.; Baker, D. R.; Pendley, S. S.; Nguyen, K.; Hurley, M. M.; Bruce, B. D.; Sumner, J. J.; Lundgren, C. A. Photocurrent Generation from Surface Assembled Photosystem i on Alkanethiol Modified Electrodes. Langmuir 2013, 29 (7), 2412−2419.

(19) López-Martínez, M.; López-Ortiz, M.; Antinori, M. E.; Wientjes, E.; Nin-Hill, A.; Rovira, C.; Croce, R.; Díez-Pérez, I.; Gorostiza, P. Electrochemically Gated Long-Distance Charge Transport in Photosystem I. Angew. Chem., Int. Ed. 2019, 58 (38), 13280−13284.

(20) Ciobanu, M.; Kincaid, H. A.; Jennings, G. K.; Cliffel, D. E. Photosystem I Patterning Imaged by Scanning ElectrochemicalMicroscopy. Langmuir 2005, 21 (2), 692−698.

(21) Leblanc, G.; Gizzie, E.; Yang, S.; Cliffel, D. E.; Jennings, G. K. Photosystem I Protein Films at Electrode Surfaces for Solar Energy Conversion. Langmuir 2014, 30 (37), 10990−11001.

(22) López-Martínez, M.; López-Ortiz, M.; Antinori, M. E.; Wientjes, E.; Nin-Hill, A.; Rovira, C.; Croce, R.; Díez-Pérez, I.; Gorostiza, P. Electrochemically Gated Long-Distance Charge Transport in Photosystem I. Angew. Chem., Int. Ed. 2019, 58 (38), 13280−13284.

(23) Zhao, F.; Hardt, S.; Hartmann, V.; Zhang, H.; Nowaczyk, M. M.; Rögner, M.; Plumeré, N.; Schuhmann, W.; Conzuelo, F. Light-Induced Formation of Partially Reduced Oxygen Species Limits the Lifetime of Photosystem 1-Based Biocathodes. Nat. Commun. 2018, 9 (1), 1 DOI: 10.1038/s41467-018-04433-z.

(24) Zhao, F.; Plumeré, N.; Nowaczyk, M. M.; Ruff, A.; Schuhmann, W.; Conzuelo, F. Interrogation of a PS1-Based Photocathode by Means of Scanning Photoelectrochemical Microscopy. Small 2017, 13 (26), 1−8.

(25) Buesen, D.; Hoefer, T.; Zhang, H.; Plumeré, N. A Kinetic Model for Redox-Active Film Based Biophotoelectrodes. Faraday Discuss. 2019, 215 (i), 39−53.

(26) Mukherjee, D.; May, M.; Vaughn, M.; Bruce, B. D.; Khomami, B. Controlling the Morphology of Photosystem I Assembly on Thiol-Activated Au Substrates. Langmuir 2010, 26 (20), 16048−16054.

(27) Qin, X.; Suga, M.; Kuang, T.; Shen, J. R. Structural basis for energy transfer pathways in the plant PSI-LHCI supercomplex. Science 2015, 348 (6238), 989−995.

(28) Robinson, M. T.; Cliffel, D. E.; Jennings, G. K. An Electrochemical Reaction-Diffusion Model of the Photocatalytic Effect of Photosystem i Multilayer Films. J. Phys. Chem. B 2018, 122 (1), 117−125.

(29) Ciesielski, P. N.; Cliffel, D. E.; Jennings, G. K. Kinetic Model of the Photocatalytic Effect of a Photosystem i Monolayer on a Planar Electrode Surface. J. Phys. Chem. A 2011, 115 (15), 3326−3334.

(30) Caterino, R.; Csiki, R.; Lyuleeva, A.; Pfisterer, J.; Wiesinger, M.; Janssens, S. D.; Haenen, K.; Cattani-Scholz, A.; Stutzmann, M.; Garrido, J. A. Photocurrent Generation in Diamond Electrodes Modified with Reaction Centers. ACS Appl. Mater. Interfaces 2015, 7 (15), 8099−8107.

(31) Milano, F.; Ciriaco, F.; Trotta, M.; Chirizzi, D.; De Leo, V.; Agostiano, A.; Valli, L.; Giotta, L.; Guascito, M. R. Design and Modelling of a Photo-Electrochemical Transduction System Based on Solubilized Photosynthetic Reaction Centres. Electrochim. Acta 2019, 293, 105−115.

(32) Manocchi, A. K.; Baker, D. R.; Pendley, S. S.; Nguyen, K.; Hurley, M. M.; Bruce, B. D.; Sumner, J. J.; Lundgren, C. A. Photocurrent Generation from Surface Assembled Photosystem i on Alkanethiol Modified Electrodes. Langmuir 2013, 29 (7), 2412−2419.

(33) Gordiichuk, P.; Pesce, D.; Ocampo, O. E. C.; Marcozzi, A.; Wetzelaer, G. J. A. H.; Paul, A.; Loznik, M.; Gloukhikh, E.; Richter, S.; Chiechi, R. C.; Herrmann, A. Orientation and Incorporation of Photosystem I in Bioelectronics Devices Enabled by Phage Display. Advanced Science 2017, 4 (5), 1−7.

(34) Ciornii, D.; Kölsch, A.; Zouni, A.; Lisdat, F. A Precursor-Approach in Constructing 3D ITO Electrodes for the Improved Performance of Photosystem I-Cyt c Photobioelectrodes. Nanoscale 2019, 11 (34), 15862−15870.

(35) Forzani, E. S.; Zhang, H.; Nagahara, L. A.; Amlani, I.; Tsui, R.; Tao, N. A Conducting Polymer Nanojunction Sensor for Glucose Detection. Nano Lett. 2004, 4 (9), 1785−1788.

(36) Qiu, X.; Castañeda Ocampo, O.; De Vries, H. W.; Van Putten, M.; Loznik, M.; Herrmann, A.; Chiechi, R. C. Self-Regenerating Soft Biophotovoltaic Devices. ACS Appl. Mater. Interfaces 2018, 10 (43), 37625−37633.